Engineering Journal issn: 0125-8281

Article

Development of Data Acquisition Technique for Inspection of Pipes in Vessel using Gamma Scanning Coupled with Computed Tomography

Dhanaj Saengchantr[1,2,a], **Somyot Srisatit**[2,b,*], **and Nares Chankow**[2,c]

1 Thailand Institute of Nuclear Technology, Ongkharak, Nakornnayok, 26120, Thailand
2 Department of Nuclear Engineering, Faculty of Engineering, Chulalongkorn University, Bangkok 10330, Thailand
E-mail: [a]dhanaj@tint.or.th, [b]somyot.s@chula.ac.th (Corresponding author), [c]naresck@yahoo.com

Abstract. This study proposes the data acquisition technique for on-line inspection of the pipe installed inside closed vessels through a laboratory model. The technique was based on transmission of gamma radiation that projected onto the radiation detectors. Laboratory model composed of four vertical pipes with different size installed inside the top opened tank. The proposed acquisition technique allowed the scanning with a few number of detectors to complete the projection as stated in Computed Tomography algorithm. Projected data were computed and reconstructed using filtered back projection algorithm and displayed in two dimension image. The simulation using Monte Carlo for N-Particle computer code (MCNP) was presented in this paper based on theoretical algorithm to be regarded as a reference result. The comparison between experimental results and simulation result showed a good agreement to each other. This technique could be extended to inspect integrity structure of pipe in vessels in petroleum and petrochemical in field work.

Keywords: Industrial computed tomography, vessel inspection, gamma scanning, pipe in vessel, on-line inspection.

ENGINEERING JOURNAL Volume 23 Issue 2
Received 24 March 2018
Accepted 4 January 2019
Published 31 March 2019
Online at http://www.engj.org/
DOI:10.4186/ej.2019.23.2.85

DOI:10.4186/ej.2019.23.2.85

1. Introduction

An online inspection of distillation column is the method to investigate the abnormality inside the distillation column, mainly in petroleum and petrochemical plants. Internal structure of distillation column composed of various structure such as piping, trays distillation, packing distillation, chimney pipes, etc. In conventional scanning, gamma scan played dominant roles since the operation was simple and easy in terms of operation and management. However, the scanning results from gamma scan were not simple as its operation. They were displayed in a format of x-y line graph and only experienced personnel can interpret them precisely, nevertheless, doubts from line graph still remained in many cases [1, 2].

Finding the method to incorporate with the accuracy of scanning result interpretation in the doubt area is challenges. Industrial Computed Tomography (ICT) technique is selected by its benefits of results representation i.e. two dimension image reconstruction. Plant inspectors have tried to apply ICT to the petroleum and petrochemical industries. The simulation software, Monte Carlo for N-Particle (MCNP), was used to simulate a transmission of gamma rays through the interested objects and reconstructed image [3]. The designed system composed of detectors and radiation source arranged until the pattern were recognized in form of 3rd and 4th generation CT projection system. Together with simulation, experiment in laboratory scale was also presented. The image reconstructed results showed good agreement between simulation and experiment [4-6]. Not only gamma radiation that had been used but also x-ray was used in ICT to investigate the efficiency of packing in a distillation process [7-9]. These results implied that, there is a possibility to apply ICT algorithm in inspection of any medium when the scanning system is applicable. The equipment used in this study composed of uncollimated 11 Sodium Iodine detectors (NaI) and Cesium-137 (Cs-137) gamma radiation source. They were arranged until it covers the area of interest inside the medium and configured as a fan-beam arrangement. The laboratory model of vessel is top opened tank with a diameter of 800 mm which installed steel pipes inside. Each pipe has diameter of 152.4 mm (6”), 101.6 mm (4”), 76.2 mm (3”) and 114.3 mm (4.5”) located at a certain position.

In principle, data acquisition for 3rd generation fan-beam projection is straight forward by retaining radiation source and set of detectors along periphery of object. This is possible when the operation has been done in the laboratory. However, if it has to be performing in the field work, rotation of equipment may not be possible, thus data acquisition technique becomes an important issue to fulfill the operation as closed to the theoretical as possible. This study explained the data acquisition pattern which allowed moving radiation source and detectors independently such that the rotation is not an issue.

2. Methodology

2.1. Data Acquisition System

The data acquisition system composed of 12 channels radiation counter connected to NaI detectors that had been calibrated until acquired signals from all detectors were giving result as closed to each other as possible. The radiation counter was connected to the PC through serial communication with parameters as specified in user manual from manufacturer. Sampling rate of 1 sec was specified to the radiation counter to generate the counting output package from all detectors every 1 second. This signal generation shall be regarded as real time clock for the counting system in PC software as well.

2.2. Image Reconstruction Algorithm

The system was setup as a fan beam projection such that the gamma radiation interacts with detectors in the manner of fan beam projection. In fact, all source and detectors were not well collimated, hence scattering radiation also contributed the data as well. However, regardless to the scattered radiation, the data acquired from the measurement can be reconstructed using conventional fan beam algorithm. In such a case, linear interpolation in between detectors can be incorporated.

The image reconstruction for fan beam can be considered by the transformation from Cartesian coordinate into the polar coordinates [10, 11]. Figure 1 shows projection annotations of fan beam. Let the shape $A\hat{S}B$ represent the fan beam rays from the radioactive source (S) which is installed with a distance D measured from center of the system. The interested information will be acquired from the detector installed

between arcs AB with the equiangular installation of α. Assume that the main beam line represents the reference angle from y-axis when source is rotated by the angle of β.

$$\theta = \beta + \alpha \tag{1}$$

$$\rho = D\sin\alpha \tag{2}$$

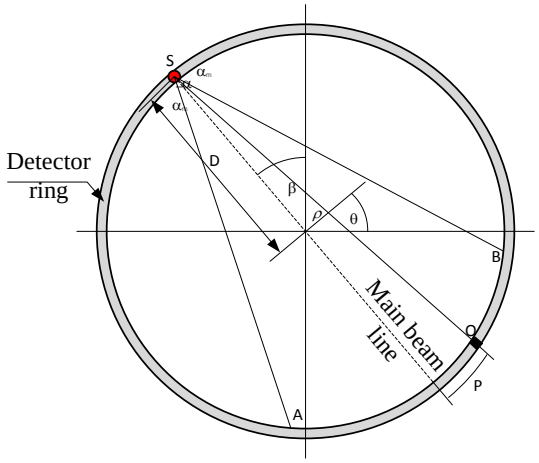

Fig. 1. Fan beam projection system.

By converting from Cartesian coordinate to polar coordinate,

$$\rho = x\cos\theta + y\sin\theta \tag{3}$$

Apply (2) and (3) to obtain the function that represents the individual ray sum when angle of interest of detectors are bounded by $-\alpha_m$ to $+\alpha_m$, $f(x, y)$ can be obtained and apply in Radon transform by

$$f(x,y) = \frac{1}{2}\int_0^{2\pi}\int_{-\alpha_m}^{\alpha_m} g(D\sin\alpha, \beta+\alpha)\delta(r\cos(\beta+\alpha-\phi) - D\sin\alpha)D\cos\alpha \mathrm{d}\alpha \mathrm{d}\theta \tag{4}$$

2.3. Scanning Pattern

In this study, the laboratory model with installed pipes inside is illustrated in Fig. 2 with its dimension and location. The PVC blocks were installed at the periphery of model to fix the position of detectors at certain point. As its allowance space, each detector pitch was assigned at angle 7.5 degree different. Hence, for 360 degree surrounded the tank model, 48 PVC blocks were installed. The scanning pattern proposed in this study will be implemented with 360 degree scanning by moving radiation source in every position of PVC block such that 48 projections were required. Since the numbers of detector used in this study have only 11 detectors, scanning to fulfill the requirement of fan-beam that covered all interesting area, arrangement of 11 detectors were designed. By simulating results from MCNP, 21 detectors provided a satisfactory result for each projection. To fulfill the requirement, two halves of scanning was designed. Consequently, 96 projections for reconstruction were implemented.

Proposed scanning pattern is illustrated in Fig. 3, the detectors were placed as half arc with same center against location of radiation source to collect the first half of projection when the radiation source is placing at position number 25. Carefully notice that, it is possible to move radiation source once to obtain the second half of projection when the radiation source is placing at position number 35. This shortens the time for just move only radiation source once while two scanning were done. To move forward and look like it is rotating, the first detector was moved to end of detector in row and repeat the same step by moving steps source to two positions. The movement goes along until the required 96 profiles are achieved.

DOI:10.4186/ej.2019.23.2.85

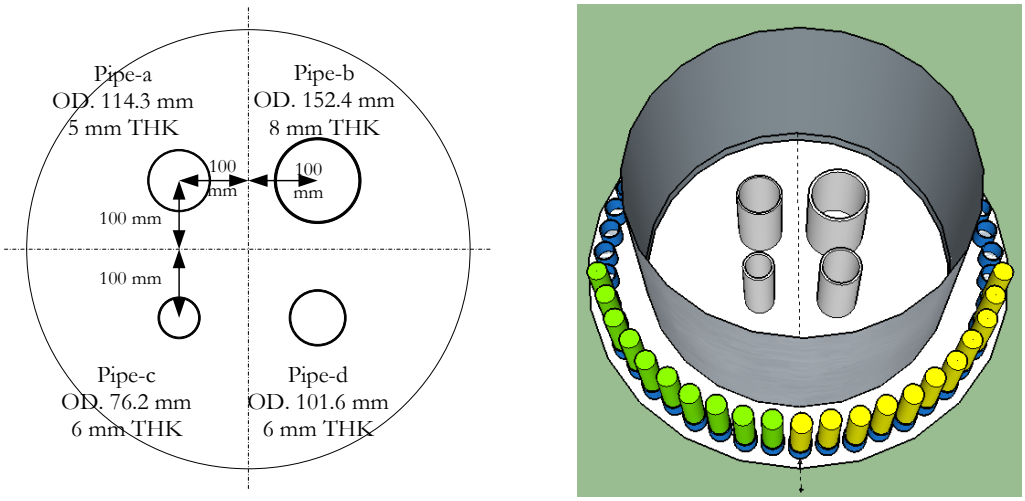

Fig. 2. Pipes arrangement inside the top open tank 800 mm in Dia.

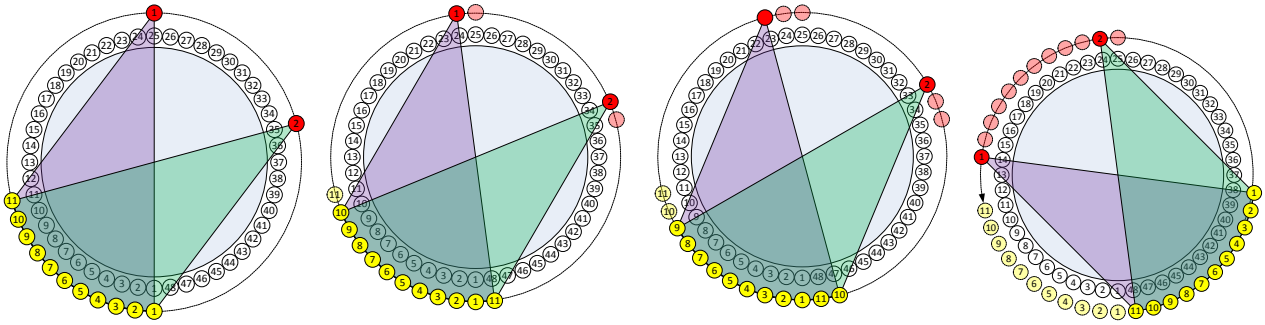

Fig. 3. Projection pattern proposed to scan in laboratory model. The purple shading represent scanning of first half while green shading represent scanning of second half.

2.4. Calibrations

The calibration was done by adjusting available parameters, i.e. High Voltage (HV), Lower Level Discrimination (LLD) and Upper Level Discrimination (ULD). The LLD was setting until the measured signal had overcome the background radiation (noise and Compton scattering). The detectors were tested with Cs-137 in order to determine the energy peak of 662 keV and set the LLD until the Compton scattering low energy were cut at 500 keV, approximately. Setting up ULD was opened since the radiation of higher energy played less dominant influence to the measurement data. Lowest count from one detector was selected as a reference detector and adjusted others detector's HV until the radiation count became closed to reference detector. This is the most important process since all detectors must be able to measure as a compatible to each other. If the system was not well calibrated, mess up reconstructed image would come.

Procedures to calibrate the system are displayed as diagram in Fig. 4. Two distance positions from source to detectors were selected as "near field" and "far field" in order to compare and to adjust HV and LLD. Near field refers to position where the detector is placing close to the radiation source. Far filed refers to the position where the detector is placing far from the radiation source. Both reference detector and calibrating detector are placing at the same time in either far or near field in order to compare and

adjust the value of calibrating detector to have value as close to the reference detector as possible. All detectors must be calibrated until it has almost the same efficiency as closed to each other in both near field and far field. The calibration procedures are as follow:

(a) Place reference detector at position called "near field" and place calibrating detector at another side of near field

(b) Measure the radiation count from gamma radiation source, adjust the HV or LLD until the radiation count of calibrating detector has the same value compared to the reference detector

(c) Move both reference detector and calibrating detector to position called "far field" and observe the radiation counting value, adjust the parameters if there is a big deviation

(d) Change the calibrating detector and repeat step (a) until all detectors are calibrated

It is necessary to use two positions "near and far field" instead of single point in order to observe the efficiency of detector when it detects high and low radiation because some detector has poor efficiency but it becomes over sensitive when receive high radiation. All detectors must be compromised to provide the good image.

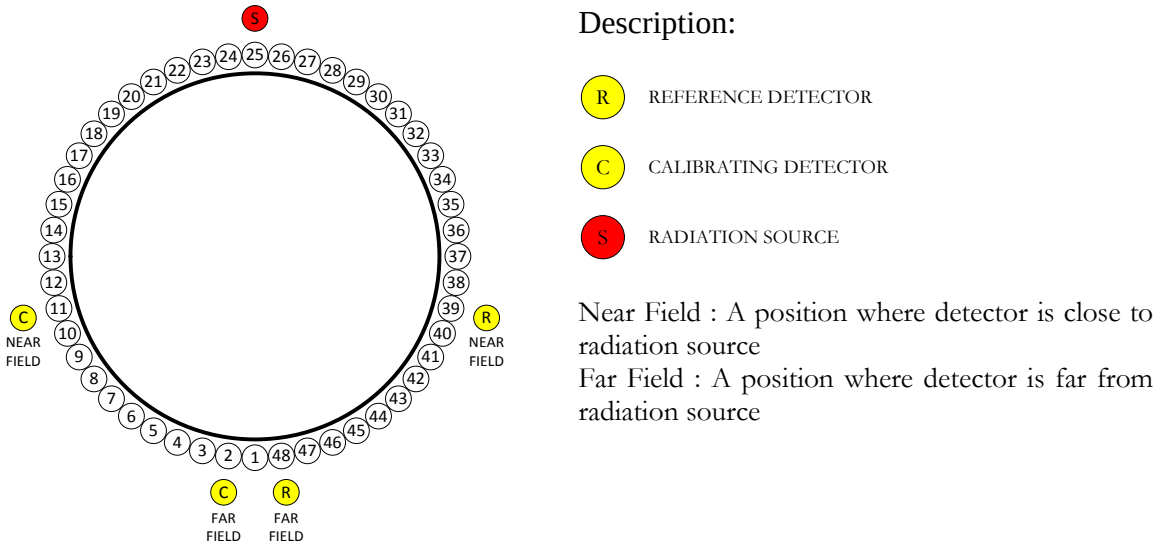

Fig. 4. Calibration positioning of reference detector and calibrating detector.

3. Experiments

This section provides experiments which had been done in this study. It composed of two parts i.e. simulation by MCNP and experiment by perform a scanning as describes in scanning pattern section. All equipment was well calibrated until all detectors generated output with almost the same efficiency to each other.

3.1. MCNP Simulation Studied Case

3.1.1. Simulation of system

The MCNPx is computer code used in both neutrons transportation and photon transportation. In this study, photon transportation is considered. The pulse height tally function F8 was used to collect information of interacted photons to detectors which can be regarded as a physical energy deposition to detectors [12, 13]. Simulation was configured by placing detectors against the radiation source such that the configuration of system is formed in fan beam as indicated in Fig. 5. In simulation the computer code generated 10^8 photons to simulate the transportation from radiation source (red circle) to the detectors (blue circle). The photons emitted from source interacts with the medium and finally either absorbed in the medium or absorbed in detectors. The interested results were the value of photons reached the detectors.

DOI:10.4186/ej.2019.23.2.85

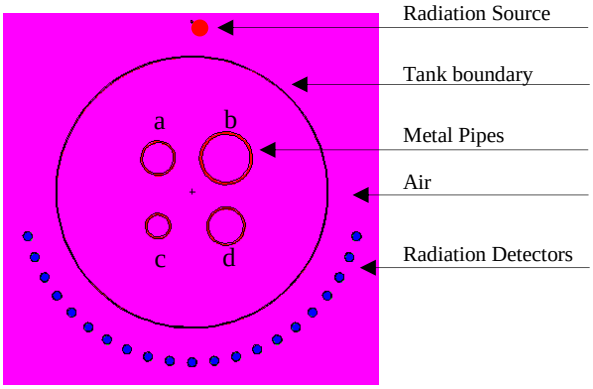

Fig. 1. System configuration generated by MCNP computer code.

3.1.2. MCNP modeling

The modelling of gamma radiation source, Cs-137 and radiation detector, NaI are displayed in Fig. 6 below. The radiation source, exclude stainless steel container is size of 6 mm in diameter and 7 mm in height. With its container, the diameter is approximately 10 mm in diameter and 7.5 mm in height. In practical, the radiation source is installed inside the source holder for safe operation.

The radiation detector is a composition of Sodium-Iodine (NaI). It composed in a form of scintillation crystal with size of 25.4 mm in diameter and 25.4 mm in height. The crystal is covered by aluminum cladding, approximately 200 mm in length; with electronics components such as a photo multiplying tube, anodes, etc. installed inside the aluminum cladding as indicate in Fig. 6. Photon energy emitted from radiation source was setting to 0.662 MeV and its spectrum distribution is displayed in Fig. 7 below. The bins selected from 0.5 MeV up to 1.0 MeV were taken into account to avoid the Compton scattering at lower energy.

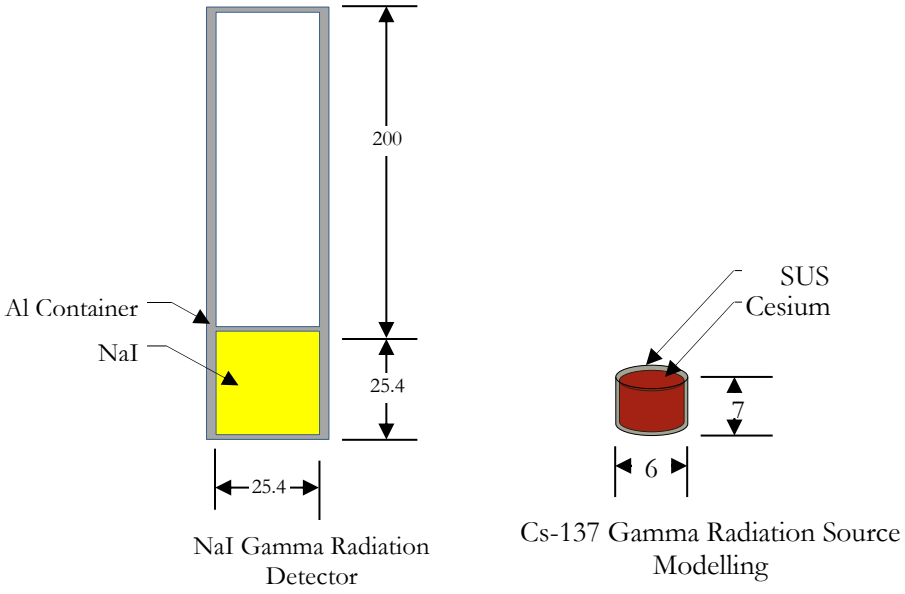

Fig. 6. Modelling of Gamma Radiation Source and Detector (units are in mm).

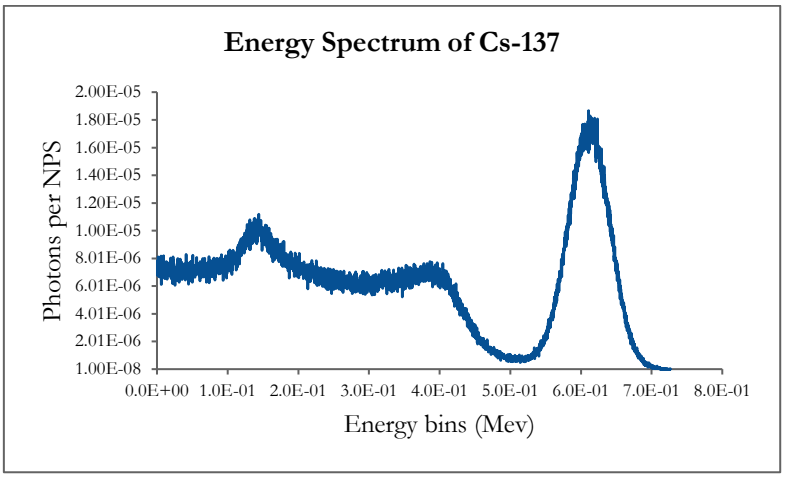

Fig. 7. Simulated Photon Energy Spectrum Distribution by MCNPx.

3.2. Experimental of Studied Case

The experiment was done through the steps as explained in section 2.3 scanning pattern. Table 1 provides example of system movement sequences. A positioning of the system is indicated in Fig. 8 below.

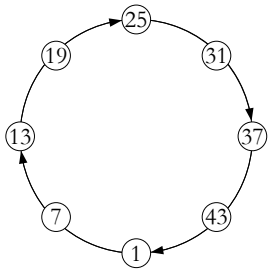

Fig. 8. System positioning for detectors and source.

Table 1. Example of detectors and source moving sequences.

Step	S	D1	D2	D3	D4	D5	D6	D7	D8	D9	D10	D11
1	25	1	2	3	4	5	6	7	8	9	10	11
2	35	1	2	3	4	5	6	7	8	9	10	11
3	24	1	2	3	4	5	6	7	8	9	10	48
4	34	1	2	3	4	5	6	7	8	9	10	48
5	23	1	2	3	4	5	6	7	8	9	47	48
.	.	.	.	.	.	.	.	.	.	.	.	.
.	.	.	.	.	.	.	.	.	.	.	.	.
.	.	.	.	.	.	.	.	.	.	.	.	.
90	39	5	6	7	8	9	10	11	12	13	14	15
91	28	5	6	7	8	9	10	11	12	13	14	4
92	38	5	6	7	8	9	10	11	12	13	14	4
93	27	5	6	7	8	9	10	11	12	13	3	4
94	37	5	6	7	8	9	10	11	12	13	3	4
95	26	5	6	7	8	9	10	11	12	2	3	4
96	36	5	6	7	8	9	10	11	12	2	3	4

S : referred Radiation Source
Dx : referred Radiation Detector Number 1-11

DOI:10.4186/ej.2019.23.2.85

4. Results and Discussion

This section provides simulation results as well as experimental results. The results are compared and discussed.

4.1. Simulation Result

The simulation results are illustrated in Fig. 9. Reconstructed image clearly showed the location of four black circles which represented four installed pipes with different size. The line profiles were plotted between gray value at each pixel along the coordinate x, y where x is varied while y is constant at 240 and 360 as indicated in Fig. 9.

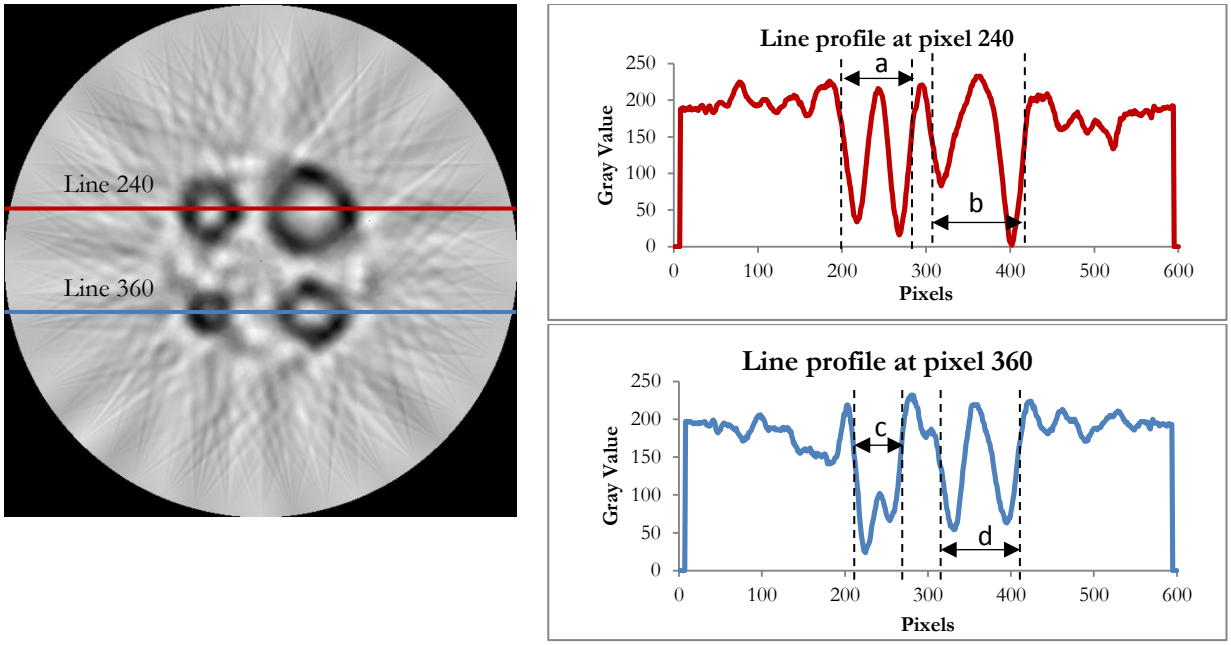

Fig. 9. System positioning for detectors and source.

The results marked as a, b, c and d were a pixel distance which will be used in pixel calibration where "a" is regarded as a reference size. Table 2 showed the pixel calibrated values where Px-1 and Px-2 are read out from graph at dotted line location. The error determined by

$$\%error = \left| \frac{Actual\ \ Size - Measured\ \ Size}{Actual\ \ Size} \right| \times 100 \tag{5}$$

Table 2. Pixel calibration and sizing of pipes from simulation results.

Pipe	Px-1 (pixels)	Px-2 (pixels)	Px2 – Px1 (pixels)	Measured Size (mm)	Actual Size (mm)	error (%)
a*	200	284	84	114.3	114.3	0.0
b	304	415	111	151.0	152.4	0.9
c	213	266	53	72.3	76.2	5.4
d	317	400	83	112.9	101.6	11.2

*Reference pipe.

The calibration factor is determined by considering the factor of reference pipe, i.e. pipe a. Factor from pixels different is calculated and obtained value is 1.361. The biggest error was 11.2% from observation of pipe d.

4.2. Experimental Result

The experimental results are illustrated in Fig. 10 below. By measure pixels and pixels different as the same way of simulation results in 4.1, Table 3 illustrated the measured pipes size using calibration factor from simulation (1.361) as well as their percent error.

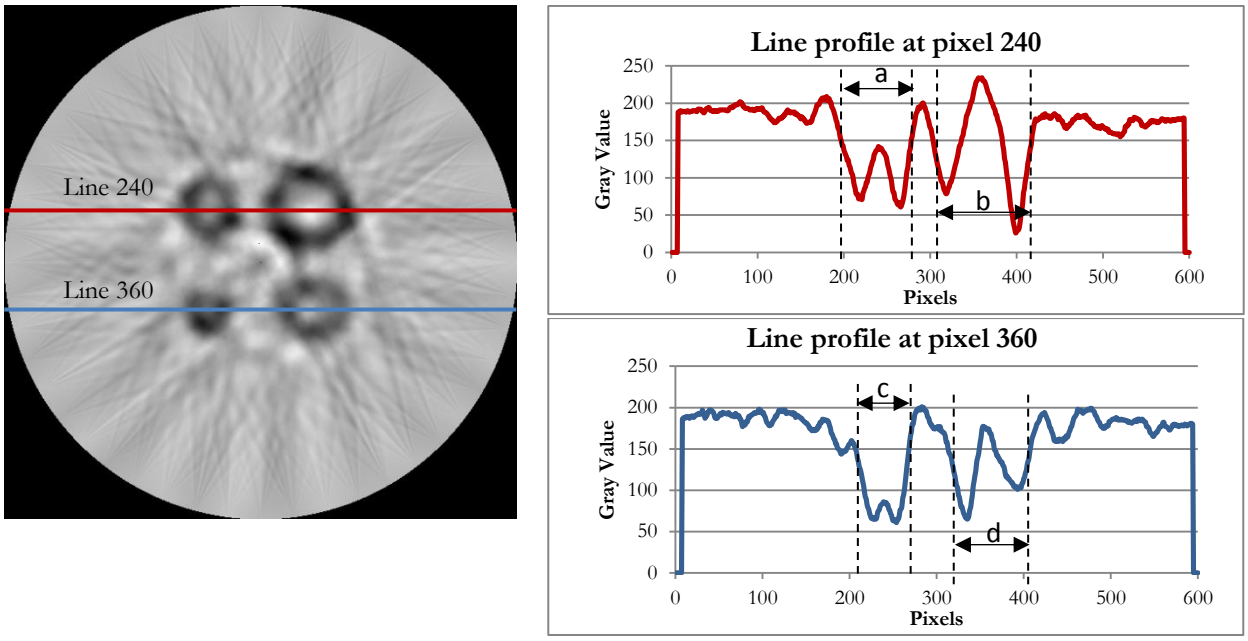

Fig. 10. System positioning for detectors and source.

Table 3. Pixel calibration and sizing of pipes from experimental results.

Pipe	Px-1 (pixels)	Px-2 (pixels)	Px2 – Px1 (pixels)	Measured Size (mm)	Actual Size (mm)	error (%)
a*	195	279	84	114.3	114.3	0.0
b	305	415	110	149.7	152.4	1.8
c	209	266	57	77.6	76.2	1.8
d	318	405	87	118.4	101.6	16.5

The experimental results show good agreement compared to the simulation. However, the percentage error of pipe-d seems to be going bigger than those observed in simulation. By observing from a gray value in experimental results of pipe-d, the ellipsoid-like shape makes wider length when measured in horizontal direction and shorter length when measured in vertical direction. The same phenomenon occurred when measured in pipe-a as well. The ellipsoid-like shape of pipe-a and pipe-d was affected by pipe-b since its thickness reached the half value layer of steel when using Cs-137, hence the source strength in experiment was not sufficient to overcome the shielding effects from thickness of pipe-b. As a result, the vertical measurements diameter of pipe-a was increased whereas the vertical measurements of pipe-d were reduced. Table 4 illustrates the measured of diameter of each pipe in both vertical and horizontal directions. The average value of vertical and horizontal measurements minimized the error of pipe-d, obviously. However, errors of pipe-a through pipe-c were slightly increased due to the ellipsoid-like shape effects.

DOI:10.4186/ej.2019.23.2.85

Table 4. Pixel calibration and sizing of pipes from experimental results.

Pipe	Horizontal Measurement (mm)	Vertical Measurement (mm)	Average Size (mm)	Actual Size (mm)	error (%)
a*	114.3	118.2	116.3	114.3	1.7
b	149.7	148.5	149.1	152.4	2.2
c	77.6	70.9	74.3	76.2	2.6
d	118.4	95.9	107.2	101.6	5.5

4.3. Comparison between Simulation and Experimental Results

Comparison of line profile number 240 and 360 between simulation and experimental results are illustrated in Fig. 11. The experiment shows some distortion in both line profiles, however the location of all pipes are consistent to each other. However, since the detectors and radiation source were not collimated, interference from scattering radiation assisted the signal and produces some distortion to the image.

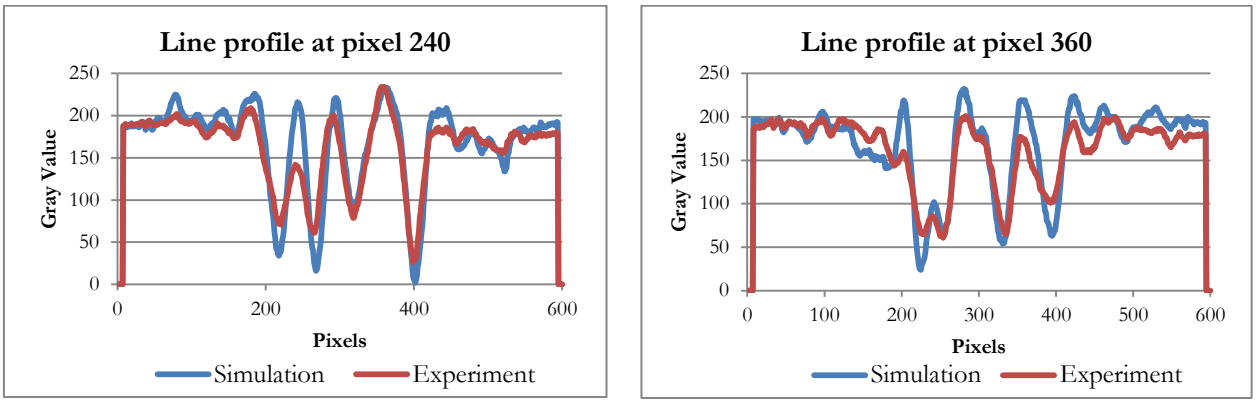

(a) (b)

Fig. 11. Profile number 240 and 360 comparison between simulation and experimental results.

5. Conclusion

This study shows the capabilities of applying the industrial computed tomographic technique into cross-section gamma scanning using simple system. The reconstructed images showed good agreement between simulation and experimental results. It means that if all system were well calibrated, the scanning results will provide satisfactory information of the medium in phantom. The calibration was the most important part of this technique since all detectors must be calibrated with the reference detector and must be able to show that all of detectors have equivalent efficiencies. If the calibration was not well established, reconstructed image became fuzzy and was not possible to represent the medium inside the interesting phantom. The proposed scanning pattern was well established since the reconstructed image provided all needed information of medium inside the phantom. In this study, the integrity of each pipe together with their sizing was the issues of interest. However, these scanning results could not communicate their thickness or corrosion of any pipes. It can be seen that the proposed pattern did not based on rotation of equipment; instead, it depends on the positioning of detectors and radiation source. Thus, freely moved allows the scanning to avoid the obstructed object such as structure's support of pipe which externally installed on vessels. One more issue to be kept into account is the post data processing since the data acquired from scanning pattern is complicated and must be rearranged until it met the requirement with fan-beam projection algorithm. Missed rearrangement of acquired data also generated the fault reconstructed image.

Consider the reconstructed image of simulation and experimental results, it can be concluded that all pipes were detected from both images. However, smallest pipe diameter of 76.2 mm. was not clear detection in experimental results compared to the simulation results. The percentage error from sizing of

pipes could also be reduced by consider pixels calibration in more than one direction, in this study two direction i.e. vertical and horizontal pixel profile plotting were done such that the biggest error was compromised from 16.5% to 5.5%

Acknowledgement

This research was funded by Thailand Institute of Nuclear Technology (Public Organization) (TINT) on all equipment and experimental facilities. The author gratefully thanks to Associate Professor Somyot Srisatit and Associate Professor Nares Chankow who provided expertise that greatly assisted this research to the satisfactory results. I also would like to thanks the Gamma Scanning Team of TINT for their encouragement and technical supports on experiments in laboratories.

References

[1] J. S. Charlton, *Radioisotope Techniques for Problem-Solving in Industrial Process Plants*. Springer, 1986.
[2] K. B. Swapan, "Trouble shooting of column operation using gamma scanning technique," in *National Seminar & Exhibition on Non-Destructive Evaluation (NDE)*, 2011, p. 323-325.
[3] Los Alamos National Laboratory, *MCNP—A General Monte Carlo N-Particle Transport Code, Version 5*. 2003, vol. 1-3.
[4] J. Kim, "Development of gamma-ray tomographic system for industrial plant inspection," dissertation, Korea Advanced Institute of Science and Technology, Daejeon, Republic of Korea, 2011.
[5] J. Kim, S. Jung, J. Moon, T. Kwon, and G. Cho, "Monte Carlo simulation for design of industrial gamma-ray transmission tomography," *Progress in Nuclear Science and Technology*, vol. 1, pp. 263-266. 2011.
[6] J. Kim, S. Jung, J. Moon, T. Kwon, and G. Cho, "Industrial gamma-ray tomographic scan method for large scale industrial plants," *Journal of Nuclear Instrument and Methods in Physics Research*, vol. 640, no. 1, pp. 139-150, 2011.
[7] D. Toye, P. Marchot, M. Crine, A. M. Pelsser, and G. L'Homme, "Local measurements of void fraction and liquid holdup in packed columns using X-ray computed tomography," *Chemical Engineering and Processing*, vol. 37, no. 6, pp. 511-520, 1998.
[8] Z. C. Wang, A. Afacan, K. Nandakumar, and K. T. Chuang, "Porosity distribution in random packed columns by gamma ray tomography," *Chemical Engineering and Processing*, vol. 40, no. 3, pp. 209-219, 2001.
[9] F. H. Yin, A. Afacan, K. Nandakumar, and K. T. Chuang, "Liquid holdup distribution in packed columns: Gamma ray tomography and CFD simulation," *Chemical Engineering and Processing*, vol. 41, no. 5, pp. 473-483, 2002.
[10] A. C. Kak and M. Slaney, *Principles of Computerized Tomographic Imaging*. Philadelphia: Society for Industrial and Applied Mathematics, 2001.
[11] R. C. Gonzalez and R. E. Woods, *Digital Image Processing*, 3rd ed.. 2010.
[12] C. Leroy and P.-G. Rancoita, *Principles of Radiation Interaction in Matter and Detection*. Hackensack, NJ: World Scientific, 2004.
[13] G. F. Knoll,, *Radiation Detection and Measurement*, 3rd ed. 2000, New York: Wiley, 2000.